

Timing and Climatic-driven Mechanisms of Glacier Advances in Bhutanese Himalaya during the Little Ice Age

Weilin Yang¹, Yingkui Li², Gengnian. Liu¹, Wenchao Chu³

¹College of Urban and Environmental Sciences, Peking University, Beijing 100871, China.

²Department of Geography, University of Tennessee, Knoxville, TN 37996, USA.

³Department of Earth System Science, Ministry of Education Key Laboratory for Earth System Modeling, Institute for Global Change Studies, Tsinghua University, Beijing 100084, China.

Correspondence to: Wenchao Chu (peterchuwenchao@foxmail.com)

Abstract. Mountain glaciers provide us a window into past climate changes and landscape evolutions, but the pattern of glacier evolution at centennial or suborbital timescale remains elusive, especially in monsoonal Himalayas. We simulated the glacier evolution in Bhutanese Himalaya, a typical monsoon influenced region, during the Little Ice Age (LIA) using the Open Global Glacier Model (OGGM) driven by six paleo-climate datasets and their average. Compared with geomorphologically-mapped glacial landforms, the model can well capture the patterns of glacier length change, but underestimates its amplitude. Simulation results revealed four glacial substages (1270s, 1470s, 1710s, and 1850s) during LIA in the study area. Statistically, a positive correlation between the number of glacial substages and glacier slope was found, indicating the occurrence of glacial substages might be a result from heterogeneous responses of glaciers to climate change. Summer temperature dominates the regional glacier evolution during the LIA.

1 Introduction

Mountain glaciers over high Himalayas provide us a critical window to explore the linkage between climatic, tectonic, and glacial systems (Oerlemans et al., 1998; Owen et al., 2009; Dortch et al., 2013; Owen & Dortch, 2014; Saha et al., 2018). Many scientists have investigated the glacial history for Himalayas at orbital-scale, indicating that a general trend of glacier advances is related to overall summer temperature, forced by orbitally-controlled insolation (Murari et al., 2014; Yan et al., 2018, 2020, 2021). However, latest observations with finer temporal resolution have revealed that the evolution of some glaciers in monsoonal Himalayas has suborbital-scale fluctuations, which has aroused more and more interest on exploring the mechanisms behind (Solomina et al., 2015; Peng et al., 2020).

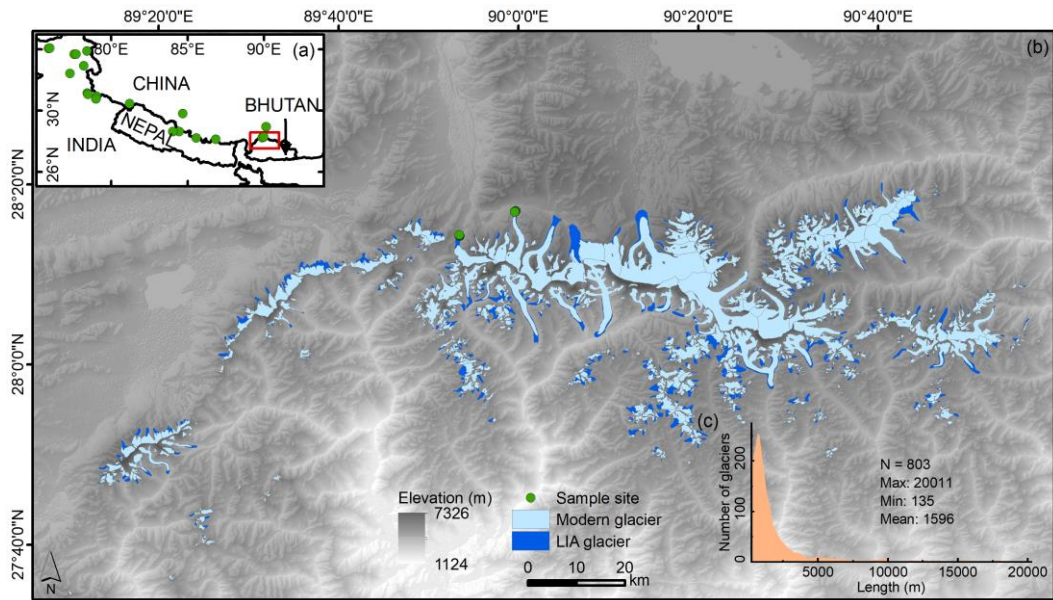
The Little Ice Age (LIA; from 1300 to 1850 CE; Grove, 2013; Qureshi et al., 2021) is the latest cooling event during the Holocene, during which most mountain glaciers advanced, forming abundant well-preserved and distinctive geomorphic landforms (Murari et al., 2014; Qiao & Yi, 2017; Peng et al., 2019, 2020). Previous studies have reconstructed the timing and extent of glacier evolution during the LIA based on field investigation, geomorphological mapping, and cosmogenic nuclide dating (Owen & Dortch, 2014 and references therein; Zhang et al., 2018a, 2018b; Carrivick et al., 2019; Qureshi et al., 2021). However, it is still unclear how many substages (glacial advances) exist during the LIA (Yi et al., 2008; Murari et al., 2014;

31 Xu & Yi, 2014), due to the post glacial degradation and the large uncertainties in the dating methods (Heyman et al., 2011; Fu
32 et al., 2013). In addition, Carrivick et al. (2019) indicated that the reconstructions using individual glaciers or a small number
33 of glaciers may be not representative for the regional average.

34 Numerical glacial modelling is a powerful way to study glacier evolution on centennial timescale (Parkes & Goosse, 2020)
35 and quantify the response of glaciers to climate change (Eis et al., 2019). It can largely alleviate the limitations in field-based
36 methods and is able to capture the glacier evolutions on regional scale. Meanwhile, the model simulations can be evaluated
37 via multiple observations to ensure the reliability. However, evaluating the simulation results is still challenging due to the
38 scarcity of the direct observational record for glacier changes during the LIA (Goosse et al., 2018).

39 Based on the above issues, this study provided a possible approach on how to bring observation and simulation together,
40 what the contribution of individual glacier to regional glacier evolution is, and how climate change drives glacier evolution
41 (Goosse et al., 2018; Carrivick et al., 2019; Peng et al., 2019, 2020). We chose a typical monsoon-influenced area, Bhutanese
42 Himalaya (BH) as an example, using the Open Global Glacier Model (OGGM) to improve our understandings on the pattern
43 of LIA glacier changes (Fig. 1). The BH (27.5~28.3°N, 89.1~91.0°E) is an east-west-trending mountain range with an average
44 elevation above 5000 m above sea level (a.s.l.), nourishing abundant high mountain glaciers (Peng et al., 2019, 2020; Fig. 1b).
45 According to the Randolph Glacier Inventory V6.2 (RGI; RGI Consortium, 2017), there exist 803 modern glaciers in BH,
46 covering an area of ~ 1233.685 km² (Fig. 1b). Fifty-seven glaciers belong to RGI13 region (Central Asia) and 746 glaciers
47 belong to RGI15 region (South Asia East). The distribution of glacier length is shown in Fig. 1c with an average length of
48 1596 m (950 m for the median value) ranging from 135 m to 20011 m. The small glaciers (length shorter than 3000 m) are
49 prevalent in BH (accounting for 88.9 %).

50 We systematically simulated the BH glacier changes during the LIA based on the climate data from six different general
51 circulation models (GCMs) and their average. The simulated glacier length changes are validated by geomorphological maps
52 and previous studies. The pattern of regional glacial evolution is compared with ¹⁰Be and ¹⁴C glacial chronologies across the
53 monsoon influenced Himalayas. The dominant climatic factors of BH glacial evolution are explored through analyzing the
54 glacier surface mass balance (SMB) changes and a series of sensitivity experiments.



55

56

57

58

59

60

Figure 1. An overview of study area and moraine sites. The red box in (a) shows the location of the study area and the green circles in (a) displays the spatial distribution of the ^{10}Be exposure dating moraines. The basic information of these moraine sites can refer to Table S1. (b) The extent of the modern glaciers (in light blue; RGI Consortium, 2017) and LIA glacier (in navy blue). The background DEM is obtained from the Shuttle Radar Topography Mission (SRTM) 90 m Digital Elevation Model v4.1 (Jarvis et al., 2008; <http://srtm.csi.cgiar.org/>). (c) The length distribution of modern glaciers.

61

2 Methods

62

2.2 Model Description

63

The OGGM (v1.50) is a 1.5D ice-flow model, able to simulate past and future mass-balance, volume, and geometry of glaciers (Maussion et al., 2019). Previous studies have confirmed a good performance of this model in simulating alpine glaciers (Farinotti et al., 2017; Pelto et al., 2020) and reproducing the millennial trend of glacial evolution in mountainous regions (Goosse et al., 2018; Parkes & Goosse, 2020). For example, OGGM has been successfully applied to simulate High Mountain Asia glaciers, including their thickness, velocity, and future evolutions (Dixit et al., 2021; Pronk et al., 2021; Shafeeque & Luo, 2021; Furian et al., 2022; Chen et al., 2022).

69

The OGGM couples a surface mass balance (SMB) scheme with a dynamic core (Marzeion et al., 2012; Maussion et al., 2019). The dynamic core adopts the shallow-ice approximation (SIA), computing the depth-integrated ice flux of each cross-section along multiple connected flowlines diagnosed by a pre-process algorithm (via geometrical centerlines). Two key parameters, the creep parameter A and the sliding parameter f_s , in the dynamic core are set to their default values ($A = 2.4 \times 10^{-24} \text{ s}^{-1} \text{ Pa}^{-3}$, $f_s = 0 \text{ s}^{-1} \text{ Pa}^{-3}$, without lateral drag). The spatial resolution (dx ; m) of the target grid is scale dependent, determined by the size of the glacier ($dx = 14\sqrt{S}$, with S representing the glacier area in km^2) but truncated by minimum (10 m) and maximum (200 m) values, respectively (Maussion et al., 2019). According to the observations, the largest simulation domain is set to 160 grid points outside the modern glacier boundaries to ensure that the domain is large enough for the LIA glaciers. If a glacier advance exceeding the domain during the simulation, we will exclude this glacier in the further analysis due to its

77

78 large simulation bias.

79 The ice accumulation is estimated by a solid precipitation scheme to separate the total precipitation into rain and snow
80 based on monthly air temperature. In this scheme, the amount of solid precipitation is computed as a fraction of the total
81 precipitation. Specially, precipitation is entirely solid if $T_i \leq T_{Solid}$ (default setting is 0 °C), entirely liquid if $T_i \geq T_{Liquid}$
82 (defaults to 2 °C) or divided into solid and liquid parts based on a linear relationship with those two temperature values. The
83 ablation is estimated using a positive degree-day (PDD) scheme (Eq. 1). Melting occurs if monthly temperature ($T_i(z)$) is above
84 T_{melt} , which is equal to -1 °C.

$$85 \quad m_i(z) = P_f P_i^{solid}(z) - \mu^* \cdot \max(T_i(z) + \beta - T_{melt}, 0) + \varepsilon, \quad (1)$$

86 where $m_i(z)$ is the monthly SMB at elevation z of month i . $P_i^{solid}(z)$ is the monthly solid precipitation, and P_f is a general
87 precipitation correction factor (default setting is 2.5). μ^* is the temperature sensitivity parameter and β is the temperature bias.
88 A residual bias term (ε) is added as a tuning parameter to represent the collective effects of non-climate factors (Marzeion et
89 al., 2012; Maussion et al., 2019). Different from the conventional PDD schemes embedded in other ice sheet models, such as
90 Parallel Ice Sheet Model (Bueler & Brown, 2009; Winkelmann et al., 2011), SICOPOLIS (Greve, 1997a, 1997b) or CISM
91 (Lipscomb et al., 2019), that assume ε and μ^* as constant values, these parameters vary with glacier in OGGM.

92 The monthly temperature and precipitation from six different GCMs (BCC, CCSM4, CESM, GISS, IPSL, and MPI),
93 covering a period from 850 CE to 2000 CE, are used to drive OGGM. These data are available in the Past Model
94 Intercomparison Project (PMIP3) and the Coupled Model Intercomparison Project (CMIP5) protocols (Schmidt et al., 2011;
95 Taylore et al., 2012; PAGES 2k-PMIP3 group, 2015) – with details listed in Goosse et al. (2018) and Table S2. The climate data
96 cannot be directly used in glacial model due to the large systematical bias of GCMs. A calibration algorithm is adopted by
97 OGGM to correct the GCMs climate data by taking the anomalies between GCMs and the Climate Research Unit (CRU) TS
98 4.01 (Harris et al., 2020) mean climate from 1961 to 1990 (Parkes & Goosse, 2020). In addition, the mean climate (MC) from
99 six different GCMs is also calculated and calibrated to drive OGGM (hereafter MC experiment) to further alleviate the climate
100 bias of each GCM. Therefore, we would focus on analyzing the results from MC experiment, but also involve some discussions
101 on the difference between MC experiment and six GCM experiments.

102 2.2 Identification of the Glacial Substages and Related Concepts

103 Similar to Goosse et al. (2018) and Parkes & Goosse (2020), we use simulated glacier length change ($\Delta L = L - L_{1950}$,
104 where L_{1950} represents the simulated glacier length at 1950) to represent glacier evolution. In order to alleviate the influence
105 of glacier size (length) to the mean value, we further convert ΔL into glacier length change ratio ($GLR = \frac{\Delta L}{L_{1950}}$). Firstly, we
106 exclude the glaciers of which the simulated lengths equal to zero at 1950 because these glaciers have large simulation biases
107 according to the observations (RGI). Then, decadal mean GLR is calculated for each glacier in order to remove the interannual

108 variabilities. Next, the Gaussian Filter (with standard deviation setting to be 3) is applied to the decadal mean GLR for each
109 glacier to extract the main oscillations. After that, we obtain the regional average GLR by averaging all glaciers' GLR (decadal
110 averaged and Gaussian Filtered) within the domain. Finally, we try to find all peaks and their corresponding times in the
111 regional average GLR timeseries based on the “findpeaks” function (with the minimum peak prominence is set to 0.2)
112 embedded in Matlab Software. Each peak found is defined as a *glacial substage* during the LIA. We name the substages from
113 new to old (LIA-1, LIA-2, LIA-3, LIA-4 and maybe more).

114 A concept related to GLR is *maximum peak GLR*, defined as the GLR when a glacier reaches its maximum peak during
115 a period. Notice that *maximum peak GLR* is different from the maximum GLR. For example, in Fig. 2d, the *maximum peak*
116 *GLR* occurs around 1270 CE rather than 1100 CE. Based on this concept, the simulated *second/third/fourth peak GLR* is
117 defined as the GLR when a glacier reaches its second/third/fourth maximum peak during a period.

118 **2.3 Spin-up, Tuning Strategy, and Experiment Design**

119 We spin-up the model to avoid the influence of the initial condition and tuned the parameter, temperature bias (β) in Eq.
120 1, to obtain a better initial condition. The β will directly regulate the initial condition (i.e., the length of initial glaciers) and
121 largely impact the *GLR* during early LIA (e.g., LIA4). Continuously forced by the climate data selected randomly from a 51-
122 year window of 875 - 925 CE, all experiments can reach their steady states after a 5000-years spin-up. In order to archive a
123 proper initial condition, we alter β from -1 to 1 °C with an increment of 0.1 °C during the spin-up period. After spin-up, we
124 model the LIA glacier changes with $\beta = 0$, forced by the past climate time series from 900 to 2000 CE. In addition, we start
125 our analysis at the year 1100 for a better display of the glacial fluctuations during the LIA (1300-1850 CE; Grove, 2013;
126 Qureshi et al., 2021).

127 The tuning procedure is based on MC experiment while six GCM experiments share the same β with MC experiment
128 during spin-up period. Our tuning strategy is threefold. First, we should ensure the regional average *GLR* is larger during LIA4
129 than LIA1 as in the observations because previous studies indicated that the majority of glaciers advanced to their LIA
130 maximum extents at the early LIA rather than the late LIA (Murari et al., 2014; Xu & Yi, 2014). Second, we need to ensure
131 the simulated *maximum peak GLR* closer to the observations. Notice that we choose to use *maximum peak GLR* because the
132 observations derived from the geomorphological mapping methods can only obtain this variable during LIA (Section 2.4).
133 Third, let more glaciers be available in the analysis as a smaller β will decrease the number of available glaciers (Fig. 2c).

134 A series of sensitivity experiments are also conducted to further validate the effect of climate changes on BH glacier
135 advances on both seasonal and annual scales. We apply a ‘constant climate scenario’, using the CRU datasets as the climate
136 forcing, and run the simulation until reaching equilibrium (here 5000 years). The window size is set to 51-year and centered
137 on t^* , the year for which the SMB scheme best reproduces the observed SMB. We set ε to 0 in Eq.1 in order to maintain the
138 contemporary glacier geometry under the contemporary climate condition. The control experiment is forced by the default

139 monthly temperature and precipitation. Keeping the same precipitation, we add a temperature bias from -1 to 1 °C with an
140 increment of 0.1 °C to the original seasonal/annual temperature to test the sensitivity of temperature on glacier evolution. The
141 similar approach is also applied to the precipitation. Holding the temperature, we adjust the precipitation from -20 to 20 %
142 with an increment of 2 % in the original seasonal/annual precipitation data.

143 2.4 Establishing Regional Chronology and Mapping LIA Glacier

144 The simulated timing and extent of glacial advances are validated with the ^{10}Be surface exposure ages and ^{14}C ages of
145 the LIA moraines and the mapped LIA glaciers over BH. Seven ^{14}C ages in monsoonal Himalaya are derived from Xu & Yi
146 (2014) and all ^{10}Be ages are recalculated using CRONUS Earth V3 online calculator with the time and nuclide-dependent
147 scaling scheme 'LSDn' (Balco et al., 2008; Lifton, et al., 2014; <http://hess.ess.washington.edu/math/>). We then adopt the
148 method advocated by Chevalier et al. (2011) and Dong et al. (2018) to exclude the potential outliers. The potential outliers are
149 defined as the ^{10}Be ages which did not overlap within 1 σ external uncertainty with others for a moraine. After removing
150 outliers, we use the oldest age of a moraine sample set to represent the moraine depositional age (Chevalier et al., 2011; Dong
151 et al., 2018; Peng et al., 2020). Five ^{10}Be ages from moraine M1 of Cogarbu valley and seven ^{10}Be ages from moraine M1 of
152 Shi Mo valley were selected to determine the regional glaciation chronology establishing in BH (Fig. 1b and Fig. S1). In
153 addition, we also chose 126 ^{10}Be surface exposure ages and 7 ^{14}C across the monsoonal Himalayas as a supplement (Fig. 1a;
154 Table S1; Xu & Yi, 2014).

155 Based on regional glacial chronology and the evidence of sediment-landform assemblages (Chandler et al., 2019), we
156 map the outermost lateral and terminal moraines in BH to represent the maximum extent of glaciers during the LIA (the
157 maximum peak GLR). These moraines are usually well-preserved with sharp crests, locating from several hundred meters to a
158 few kilometers away from the termini of modern glaciers, and damming a lake in front of modern glaciers (Qiao & Yi, 2017;
159 Zhang et al., 2018b; Qureshi et al., 2021). We use the world imagery ESRI (http://goto.arcgisonline.com/maps/World_Imagery)
160 and Google Earth high-resolution imagery to delineate the LIA moraines and outlines. However, not all LIA glaciers could be
161 identified due to the destruction of moraines. Only 408 glaciers of the 803 BH glaciers could be mapped (Fig. 1b). The length
162 of contemporary glaciers is provided in Randolph Glacier Inventory V6 datasets (RGI; RGI Consortium, 2017), and that of
163 the LIA glaciers is calculated in ArcGIS based on the main model flowline in OGGM.

164 3 Results

165 3.1 The Choice of Initial Condition

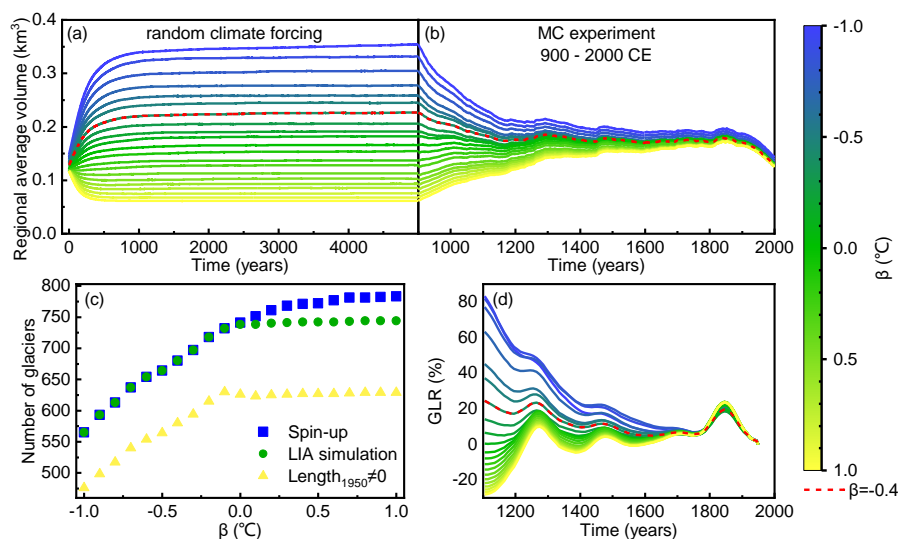
166 In order to obtain a better estimation of the initial condition, we tuned the β during the spin-up period. As shown in Fig.
167 2, β strongly influences the initial condition and thus the LIA simulation results, especially for the first 600 years (Fig. 2b).
168 With a decreased β , the regional average glacier volume increases (Fig. 2a), but the number of available glaciers (i.e., glaciers

169 which do not exceed the prescribed domain boundaries) decreases during the spin-up period (Fig. 2c). The number of available
 170 glaciers for the LIA simulation is approximately equal to that during the spin-up period, except for a reduction when β is
 171 positive (Fig. 2c). This is probably because smaller β can kick out the glaciers which would potentially suffer from large
 172 simulation bias during LIA simulation. In addition, more glaciers disappear in 1950 ($Length_{1950} = 0$; Fig. 2c) with a larger β ,
 173 consistent with our knowledge.

174 Initial condition slightly impacts the time and number of glacial substages but largely influences the strength of glacial
 175 substages (GLR) during LIA simulation (Fig. 2d; Fig. S1). Four substages occurred at ~ 1270 s (LIA-4), ~ 1470 s (LIA-3), ~ 1710 s
 176 (LIA-2) and ~ 1850 s (LIA-1) are detected under a wide range of β (from -0.7 °C to 1.0 °C) in the MC experiment. However,
 177 the number of substages become less when β is smaller than -0.7 . This is because smaller β would cause excessively large
 178 initial glaciers so that a smaller climate perturbation is not powerful enough for the glaciers to stop retreating during the early
 179 LIA period.

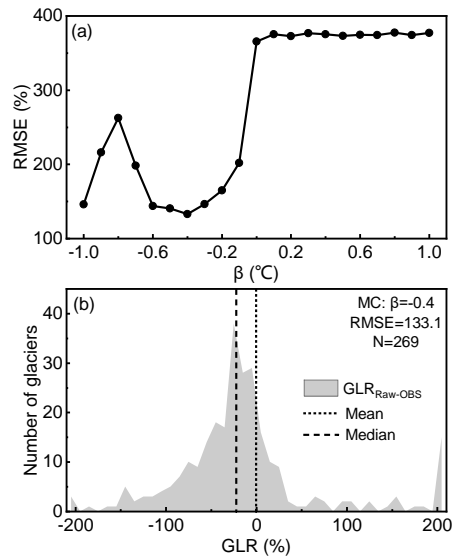
180 The GLR during the early LIA periods (LIA-4 and LIA-3) are strongly regulated by the initial condition (Fig. 2d). Smaller
 181 β will lead to a larger GLR during LIA-4 and LIA-3. According to the tuning strategies in Section 2.3, simulations with $\beta \geq -0.3$
 182 should be excluded as larger GLR must be ensured during LIA-4 than LIA-1. The Root Mean Squared Error (RMSE) of
 183 *maximum peak GLR* between the simulation and observation is smallest when $\beta = -0.4$ (RMSE = 133.1 %), though a
 184 decreasing trend is found when $\beta \leq -0.8$ (Fig. 3). However, the number of available glaciers when $\beta \leq -0.8$ is less than that
 185 when $\beta = -0.4$. Therefore, we finally choose the simulation results with $\beta = -0.4$ based on the tuning strategies.

186



187 Figure 2. (a) The regional average glacier volume during the 5000-year spin-up with various β . (b) The simulated regional
 188 average glacier volume from 900 to 2000 CE with different initial condition. (c) The number of available glaciers with various
 189 β . (d) The simulated regional average GLR from 1100 to 1950 CE.

191



192

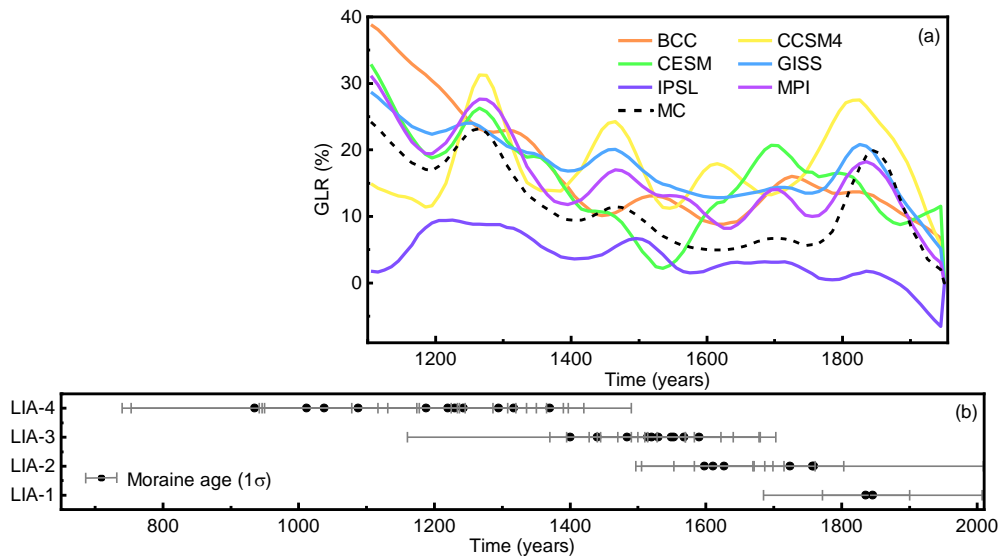
193 Figure 3. (a) The RMSE of *maximum peak GLR* between the raw simulation results and mapped LIA glaciers for the MC
 194 experiment with various β . (b) The simulation bias distribution of *maximum peak GLR* for the MC experiment with $\beta = -0.4$.

195 **3.2 The pattern of glacier changes during the LIA**

196 We would focus on the pattern of glacier changes during the LIA in MC experiment, but six GCM simulations are also
 197 shown in Fig. 4a for comparison. The simulation results in most experiments indicate four LIA glacial substages in BH, except
 198 for the CESM experiment losing LIA-3 substage. The timings of the four LIA glacial substages are 1270s (LIA-4), 1470s
 199 (LIA-3), 1710s (LIA-2), and 1850s (LIA-1) in MC experiment. These times vary slightly among the six GCM experiments,
 200 around 1230s - 1320s, 1470s - 1520s, 1620s - 1730s, 1800s - 1850s, respectively.

201 The most extensive glaciers occurred during LIA-4 in MC and six GCM experiments because our tuning strategy is to
 202 ensure larger the regional average *GLR* at the early LIA. The *second peak GLR* occurred during LIA-1 in MC experiment,
 203 similar to the results in the CCSM4, GISS, and MPI experiments but different from the results in BCC (LIA-2), CESM (LIA-
 204 2), and IPSL (LIA-3) experiments. The *third* and *fourth peak GLR* occurred during LIA-3 and LIA-2 respectively in MC
 205 experiment, also consistent with the simulations forced by CCSM4, GISS and MPI climate datasets.

206



207

208

209

210

211

Figure 4. (a) Time series of regional average *GLR* from 1100 to 1950 CE. (b) The observational timing when glaciers in the monsoonal Himalaya reached their *maximum peak GLR*. We grouped the moraine ages based on their temporal distances to each glacial substage simulated in MC experiment. The detailed information of the moraine ages measured by ^{10}Be and ^{14}C can be found in Table S1 and Xu & Yi (2014), respectively.

212

4 Discussions

213

4.1 Comparison between Simulations and Observations

214

215

216

217

218

219

220

221

222

223

224

We validated the simulation results using the moraine ages and mapped LIA glaciers (Section 2.4). The simulated regional average *maximum peak GLR* (59.9%; Fig. 3b) in MC experiment agrees well with that of mapped glaciers (60.6 %). Similarly, the simulation results in BCC (57.8 %), GISS (58.9 %) and MPI (71.0 %) experiments are also consistent with observations. Observations from adjacent regions also support the simulation results (Qiao & Yi, 2017; Zhang et al., 2018b). For example, Qiao & Yi (2017) found that the *maximum peak GLR* increased about 53.8 % during LIA in the central and western Himalayas relative to 2015. Zhang et al. (2018b) reported a 71.5 % increase of *maximum peak GLR* during LIA in the Gangdise Mountains relative to 2010, based on the glacial geomorphological maps. However, the CCSM4 (99.0 %) and CESM (80.8 %) experiments overestimated the *maximum peak GLR* while the IPSL (32.1 %) experiment underestimated it (Fig. S1). In addition, the negative bias for the median value in the simulations compared with observations is identified in the MC and six GCM experiments (Fig. 3b and Fig. S1). The difference between the mean value and median value indicates some extremums might impact the average.

225

226

227

228

229

230

The occurrence time of the *maximum peak GLR* is during LIA-4 in MC experiment, consistent with the moraine ages that the majority of glaciers advanced to their LIA maximum extents at the early LIA rather than the late LIA (Fig. 4b; Murari et al., 2014; Xu & Yi et al., 2014). Specifically, about 12 of the 30 moraine ages shows that the related glaciers reached their *maximum peak GLR* during LIA-4 compared with only 2 of them during LIA-1. However, there are still a large number of glaciers reaching their *maximum peak GLR* during LIA-3 (about 10 glaciers) and LIA-2 (about 6 glaciers). Ignoring the large uncertainties in the dating methods, the collective and individual differences in glacier changes are worth exploring. We will

231 further discuss this issue in Section 4.2.

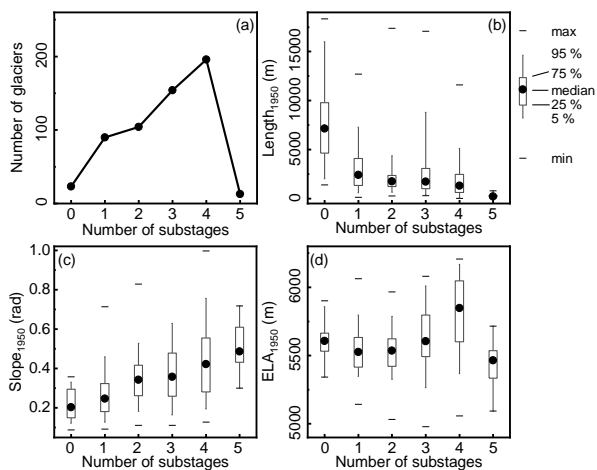
232 The simulated number of LIA substages is also comparable with observations, including some moraine dating results and
233 climatic proxy records. For example, Murari et al. (2014) and Zhang et al. (2018a) have identified four LIA moraines in
234 Bhillangana and Dudhganga valleys, Garwal Himalaya, and Lopu Kangri Area, central Gangdise Mountains, respectively. Liu
235 et al. (2017) have found at least three LIA moraines in Lhagoi Kangri Range, Karola Pass. Yang et al. (2003) found four cold
236 phases during AD 1100-1150, 1500-1550, 1650-1700, and 1800-1850 over TP and eastern China according to the proxy data
237 of paleoclimate. A regional moraine chronologies framework composed of ^{14}C , lichenometry, and cosmogenic radionuclide
238 ages found three substages during late-14th, 16th to early-18th, and late-18th to early-19th, corresponding to LIA-3, LIA-2, and
239 LIA-1, respectively (Xu & Yi, 2014). However, the divergent number of LIA substages were also confirmed by some dating
240 results and records. For example, only one moraine was dated in Cogarbu valley (1484 ± 44 CE; Table S1; Peng et al., 2019)
241 and Shi Mo valley (1514 ± 69 CE; Table S1; Peng et al., 2020), but two substages were constrained in Lato valley, Lahul
242 Himalaya (Saha et al., 2018), Langtang Khola valley, Nepal Himalaya (Barnard et al., 2006), and Gongotri Ganga valley,
243 Garhwal Himalaya (Barnard et al., 2004). By applying dendroglaciology approach, Hochreuther et al. (2015) and Bräuning
244 (2006) only detected one LIA substage in Gongpu glacier, Zepu glacier, Baitong glacier and Gyalaperi glacier, while more
245 substages were found in Lhamcoka glacier (Bräuning, 2006), Xinpu glacier (Hochreuther et al., 2015), Gangapurna glacier,
246 and Annapurna III glacier (Sigdel et al., 2020). Yi et al. (2008) identified three substages during AD 950-1820 based on 53 ^{14}C
247 dating ages.

248 4.2 Why do four LIA substages exist in BH?

249 Clearly, MC experiment and GCM experiments (excluding CESM experiment) indicate four glacial substages over BH
250 during LIA. However, due to the glacier individualities (different slopes and lengths), this does not mean each glacier in our
251 study area exists four LIA substages (Fig. 5a), consistent with the moraine dating results. Instead, it just reflects that the
252 majority of glaciers in BH have four glacial substages. For example, in MC experiment, only about 33.8 % glaciers have four
253 substages during the LIA, while the rest glaciers are with zero (4.0 %), one (15.5 %), two (17.9 %), three (26.6 %) and five
254 (2.2 %) substages. We argue that the difference in LIA substages is caused by the sensitivity of different glaciers despite many
255 studies ascribed it to the different climate conditions (Owen & Dortch, 2014; Murari et al., 2014; Saha et al., 2019). Analysis
256 found the number of glacial substages are significantly correlated to the glacier properties (glacier length and slope). The
257 glacial substage numbers have significantly positive correlation with the glacier slopes while obviously negative correlation
258 with the glacier length (Fig. 5b, c). The correlation coefficient (CC) between the number of glacial substages and glacier length
259 at 1950 is -0.31 and the CC between the number of glacial substages and glacier slope at 1950 is 0.41. Both of the CCs can
260 pass 95% significant test. However, when zooming into the main glacial substages numbers (2, 3, 4), the relationship between
261 the number of glacial substages and glacier length does not become that clear (Fig. 5b). Therefore, we argue that glacial slope

262 may dominate the glacial substage numbers during LIA (Lüthi, 2009; Zekollari and Huybrechts, 2015; Bach et al., 2018; Eis
 263 et al., 2019). The negative correlation between the glacier length and glacial substage numbers might be a result of the fact
 264 that the longer (larger) glacier has a smaller slope (CC = -0.50). Besides, analysis also suggests weak relationship between
 265 glacial substage numbers and glacial ELA (Fig. 5d).

266



267

268 Figure 5. (a) The identified glacial substages number distribution in the MC experiment. The relationship between identified
 269 glacial substages with (b) glacier length, (c) glacier slope, and (d) glacial ELA at 1950 in the MC experiment.

270

271 The occurrence time of each glacial substage also varies from glaciers, supported by the dispersal of moraine ages (Fig.
 272 4b). Notice that not all glaciers in BH reached their *maximum peak GLRs* during LIA-4, and taking a step back, even among
 273 the glaciers with the *maximum peak GLR* during LIA-4, the occurrence times are also different (Fig. 6a). Statistically, about
 274 48.1 % glaciers experienced their *maximum peak GLR* during LIA-4 followed by 36.1 % glaciers reaching their *maximum*
 275 *peak GLR* during LIA-1. Therefore, the occurrence time of *maximum peak GLR* at regional scale is associated with the
 276 occurrence time of the majority of glaciers reaching their *maximum peak GLRs*. In addition, this can in turn explain the lack
 277 of some moraines. Considering two glaciers both having four glacial substages but different occurrence times of *maximum*
 278 *GLR peak* (one at LIA-4 and another at LIA-1) during LIA, we might find 4 moraines for the glacier which reaches its *maximum*
 279 *GLR peak* at LIA-4 but only 1 moraine for the other because the first three moraines are destroyed by the last glacier advance.
 280 Similarly, this phenomenon also remains in the occurrence times of the *second/third/fourth peak GLR* (Fig. 6b-c).

281

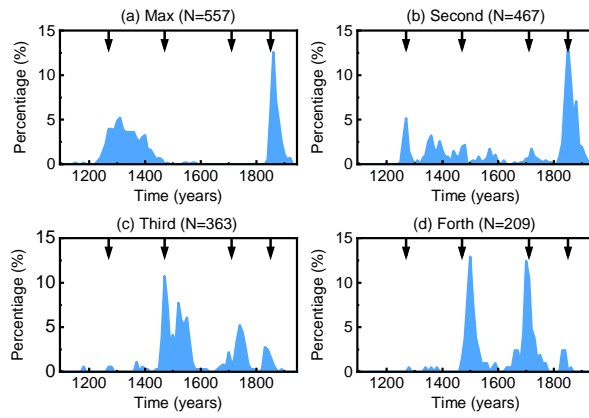


Figure 6 The percentage of the glaciers with (a) *maximum peak GLR*, (b) the *second largest peak GLR*, (c) the *third largest peak GLR*, and (d) the *fourth largest peak GLR* over time in the MC experiment. The arrows represent the time of the four glacial substages, 1270s (LIA-4), 1470s (LIA-3), 1710s (LIA-2), and 1850s (LIA-1).

In summary, four LIA glacial substages at 1270s, 1470s, 1710s, and 1850s were found in BH based on the MC experiment. The maximum glacier extent appeared during LIA-4, comparable with the moraine ages. The regional glacial evolution is a collective effect of individual glacier changes. Four substages during LIA at the regional scale does not guarantee that each individual glacier has four substages. Likewise, not all glaciers in BH reached their *maximum peak GLRs* during LIA-4. Instead, it only represents the characteristics of most typical glaciers that accounted for the vast majority of the total glaciers. This can explain why there exists four substages in regional scale in the simulation but is hard captured in the previous studies that only focus on one individual glacier, which helps us to deeply understand the relationship between regional glacial evolution and the individual glacier response to climate change.

4.3 Climate-forcing Mechanisms

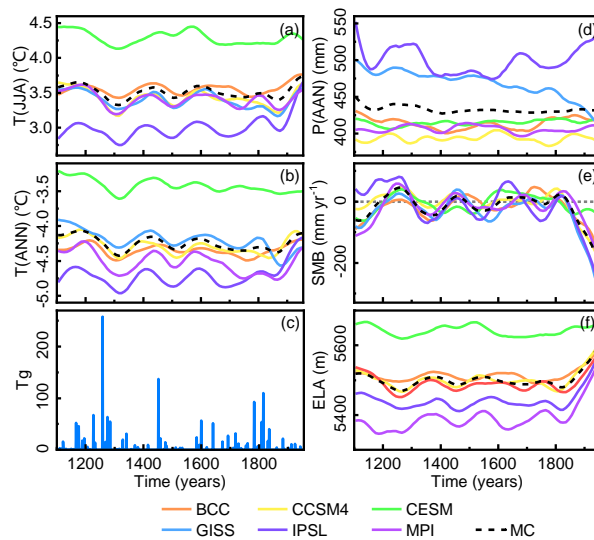
Despite we have found the regional glacial evolution is a collective effect of individual glacier changes, the dominant climatic mechanisms behind are still unclear. A better understanding of the possible forcing mechanism of regional paleoglacier fluctuations at centennial timescales benefits projecting glacier outlooks in the future (Solomina et al., 2015). However, due to the limitation of field investigations, previous studies simply ascribed the glacier change to the temperature variation in the monsoon-influenced Himalaya by comparing the regional glacial sequences with the $\delta^{18}\text{O}$ record from Greenland, Tibetan or North Atlantic (Peng et al., 2019, 2020). As the model can explicitly link the glacier changes with climate forcings (PDD scheme), it provides us an opportunity to further explore on this issue.

Our study revealed that the regional glacial fluctuations are related to the temperature changes rather than the precipitation change (Fig. 4a and Fig. 7a, b, d). Four cold intervals around 1320s, 1510s, 1760s, and 1870s in the MC experiment corresponds to LIA-4 (1270s), LIA-3 (1470s), LIA-2 (1710s), and LIA-1 (1850s), respectively. However, this signal cannot be detected in precipitation changes. Results from six GCM experiments also support this argument though with different time and strength. The four cold intervals during the LIA in BH are closely linked to four large stratospheric sulfur-rich explosive eruptions

308 events (sulfate aerosol loadings > 60 Tg; Fig. 7c; Gao et al., 2008). The beginning of oldest cold period (LIA-4) might be
 309 forced by a series of volcanic activities, including a massive tropical volcanic eruption in 1257 followed by three smaller
 310 eruptions in 1268, 1275, and 1284 (Miller et al., 2012). The volcanoes Billy Mitchell (1580), Huaynaputina (1600), Mount
 311 Parker (1641), Long Island (1660), and Laki (1783) may contributed to the cooling events during LIA-3 and LIA-2 (Jonathan,
 312 2007). The 1815 eruption of Tambora and the 1883 eruption of Krakatau are believed to promote the youngest cold period of
 313 LIA (LIA-1; Rampino and Self, 1982).

314 Although temperature determines whether BH can run into a glacial substage, precipitation still has the ability to regulate
 315 the time of glacier advancing to its maximum in a glacial substage due to the fact that SMB is determined by the combination
 316 of temperature and precipitation according to the PDD scheme (Eq. 1; Marzeion et al., 2012; Maussion et al., 2019). Positive
 317 or negative SMB determines whether a glacier advances or retreats, and the amplitude of glacier change is directly influenced
 318 by the amplitude of SMB change and the duration of the positive or negative SMB (Marzeion et al., 2012; Maussion et al.,
 319 2019; Fig. 4a and Fig. 7e). Four peaks of SMB have been found in the MC experiment, around 1260s, 1460s, 1670s and 1820s,
 320 corresponding to each substage. Stronger precipitation, associated with larger SMB, at the beginning of the cold interval will
 321 drive the glacier advance rapidly, shortening the time for it to reach its maximum extent. In addition, we also found ELA has
 322 a good correlation of the SMB, which can be used as a proxy for SMB. ELA is the elevation where accumulation equals
 323 ablation for a certain glacier (Fig. 7f; Benn & Lehmkuhl, 2000; Heyman, 2014). Four periods of ELA dropping around 1270s
 324 (-132.2 m), 1470s (-115 m), 1690s (-113.4 m), and 1820s (-112 m) are detected in the MC experiment, agreeing well with
 325 SMB change. This finding, to some extent, would benefit field investigation as paleo ELA is easily available while paleo SMB
 326 is hard to measure.

327



328

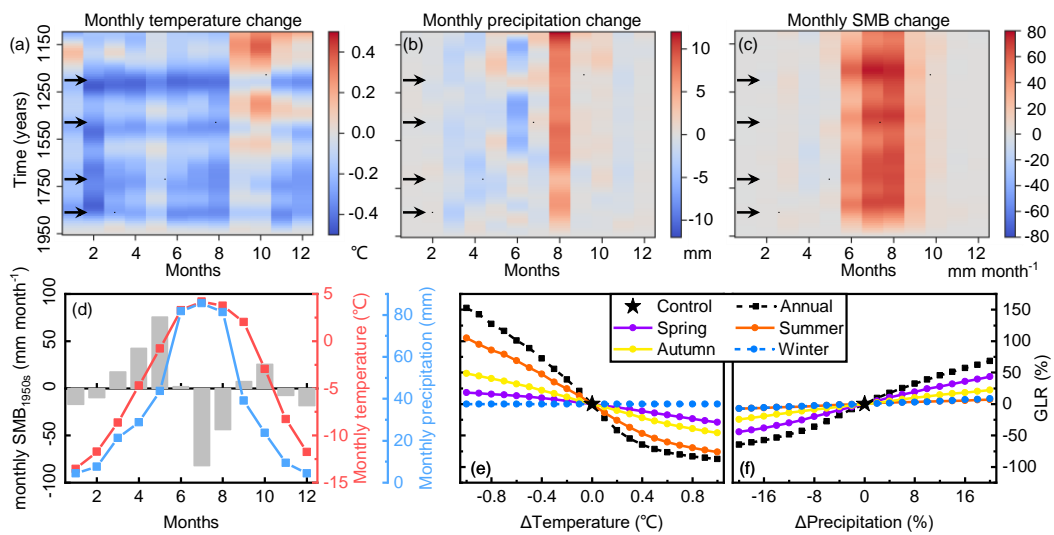
329 Figure 7. The regional average (a) summer temperature (T(JJA)), (b) annual temperature (T(ANN)), (d) annual precipitation
 330 (P(ANN)), (e) SMB, (f) ELA from 1100 to 1950 CE at a decadal timescale. (c) Global stratospheric sulfate aerosol loadings
 331 (Gao et al., 2008).

332

333 Seasonal climate is believed to have more important impacts on glacier evolutions than annual climate (Yan et al.,2020,
334 2021). We calculated the regional average monthly temperature, precipitation, cumulative SMB anomalies (relative to 1950s)
335 from 1100s to 1950s (Fig. 8a, b, and c) in the MC experiment to investigate the effect of monthly climate changes on glacial
336 fluctuation. Consistent with the Fig. 7e, four significant increasing periods of monthly SMB changes around 1270s, 1470s,
337 1710s, and 1850s are identified (Fig. 8c) as a result of monthly temperature decreasing (Fig. 8a). Monthly precipitation does
338 not show obvious change, expect for an abrupt increment in August (Fig. 8b). The abnormal increasing of August
339 precipitation is polluted by the GISS climate dataset which suffers from large precipitation bias.

340 Strong cumulative SMB change only occurs in JJA despite the temperature change almost uniformly distributes and
341 precipitation slightly variates (excluding August) throughout the year. The pattern of seasonal SMB change indicates that the
342 summer temperature might dominates the annual cumulative SMB. This is because JJA is the main ablation season of glaciers
343 in the monsoon-influenced Himalaya due to a higher temperature (Fig. 8d). A reduction of summer temperature will not only
344 decrease the number of positive degree days but also decrease the average temperature during the positive degree days,
345 resulting in the reduction in summer ablation (Eq. 1). Meanwhile, JJA is also the wettest season in the study area. **Decreasing**
346 **temperature will lead to an increasing probability of solid precipitation, enhancing the accumulation.** As the SMB is determined
347 by the sum of ablation and the accumulation, **the JJA SMB is largely increased.** However, though the temperature also decreases
348 in DJF, no more precipitation will not increase the accumulation. Therefore, the SMB change is weak.

349



350

351 Figure 8. The monthly (a) temperature, (b) precipitation, and (c) SMB changes relative to 1950s at a decadal timescale in the
352 MC experiment. The arrows in (a) – (c) represent the time of the four glacial substages, 1270s (LIA-4), 1470s (LIA-3), 1710s
353 (LIA-2), and 1850s (LIA-1). (d) the monthly temperature, precipitation, and SMB distribution in 1950s. Sensitivity of GLR to
354 annual or seasonal (e) temperature and (d) precipitation.

355

356 We also conducted a series of the sensitivity tests to examine the influence of seasonal temperature or precipitation on
357 BH glacier change (Fig. 8e, f). Glaciers retreats gradually as a response to the temperature increases or precipitation decreases.

358 The sensitivity of glaciers to temperature/precipitation (changing rates) increases with temperature/precipitation increases
359 firstly, reaches maximum at 0, and decreases after that, with an average changing rate of -160.1 %/°C for temperature and of
360 4.0 %/% for precipitation. Glaciers are most sensitive to summer temperature change with an average change rate of 110.4 %/°C,
361 followed by autumn (51.6 %/°C) and spring (25.2 %/°C). Glaciers is not sensitive to winter temperature change (0.0 %/°C),
362 supporting the results in Fig. 8c. This indicates that the temperature changes in warm seasons, especially in summer, explain
363 the most variance of the GLR changes. Fixing temperature, the sensitivity of glaciers to precipitation changes is higher in
364 spring (2.4 %/%), followed by autumn (1.1 %/%), summer (0.4 %/%) and winter (0.4 %/%). Therefore, the precipitation
365 change in spring and autumn has larger influences on glacier evolution. In order to compare the relative sensitivity of
366 temperature and precipitation to glacier change, we introduced an index $k = \frac{\Delta p}{\Delta T}$, which represents how precipitation will
367 change in response to the temperature variation (Jeevanjee and Romps, 2018). This is an index only related to the local climate
368 and is about 1.7 %/°C in the MC experiment. From our sensitivity tests, we need a $k = 53.0$ %/°C to maintain the LIA glacier
369 pattern (GLR = 60.6 %), which is much larger than local climate k , indicating the temperature dominates the LIA glacial
370 fluctuation in BH.

371 In summary, seasonal analysis and sensitivity tests indicate that the change in temperature, especially summer temperature,
372 is the dominant forcing factor for glacier changes during the LIA (sub-orbital scale) in monsoonal influenced Himalaya. In
373 contrast, the impact of precipitation change is limited. This conclusion has been drawn by Yan et al. (2020, 2021) at the orbital
374 scales, but now can be extends to the sub-orbital scale. In addition, we also found that the temperature changes during LIA are
375 closely related to volcanic activities (Gao et al., 2008; Miller et al., 2012).

376 5 Conclusions

377 We simulated the glacial evolution across BH during LIA using the coupled mass-balance and ice flow model, OGGM.
378 Compared with the geomorphological maps and moraine ages, OGGM broadly captures the pattern of glacier length change,
379 but underestimates its amplitude. The regional pattern of glacier changes is the collective effect of each glacier. The dispersal
380 of the observations could be reproduced by the model due to the individualities of each glacier. On the regional scale, four LIA
381 substages were identified at about 1270s, 1470s, 1710s, and 1850s (from LIA-4 to LIA-1) in the MC experiment. The most
382 extensive glacial advances occurred during LIA-4, consistent with regional glacial chronological and geomorphic evidence.
383 The number of glacial substages for individual glacier has a positive correlation with glacier slope. The regional glacier
384 advances are dominated by the reduction of summer ablation.

385 Although limitations still exist in the simulations, such as the application of sOGGM on amplitude of glacier changes, this
386 study presented the first simulation of sub-millennium glacial evolutions during LIA in BH using the OGGM. We found a
387 testable relationship between seasonal climate change and glacier expansion, explained the dispersal of moraine ages and
388 revealed the reasons for the four glacial substages during LIA in BH. Our findings link the limited observations with the model

389 simulations and provide important insights into the climate forcing mechanism on glacier change at centennial timescale.

390 **Code and data availability.** Code to run OGGM v1.5.0 is available at <https://zenodo.org/record/4765924#.YnYuB4dBxD8>
391 (Maussion et al., 2019).

392 **Author contributions.** Study concept devised by CW. YW performed the model runs and analysis, and wrote the original
393 draft. LY and LG reviewed and revised the paper.

394 **Competing interests.** The authors declare that they have no conflicting interests.

395 **Acknowledgments.** This work was supported by the Second Tibetan Plateau Scientific Expedition and Research (STEP; grant
396 no. 2019QZKK0205) and the National Natural Science Foundation (NSFC; grant no. 41771005, 41371082).

397 References

398 Bach, E., Radić, V., and Schoof, C.: How sensitive are mountain glaciers to climate change? Insights from a block model, *J*
399 *Glaciol.*, 64(244), 247-258, <https://doi.org/10.1017/jog.2018.15>, 2018.

400 Balco, G., Stone, J.O., Lifton, N.A., and Dunai, T.J.: A complete and easily accessible means of calculating surface exposure
401 ages or erosion rates from ^{10}Be and ^{26}Al measurements, *Quat. Geochronol.*, 3, 174-195,
402 <https://doi.org/10.1016/j.quageo.2007.12.001>, 2008.

403 Barnard, P.L., Owen, L.A., Finkel, R.C., and Asahi, K.: Landscape response to deglaciation in a high relief, monsoon-
404 influenced alpine environment, Langtang Himal, Nepal, *Quaternary. Sci. Rev.*, 25, 2162-2176,
405 <https://doi.org/10.1016/j.quascirev.2006.02.002>, 2006.

406 Barnard, P.L., Owen, L.A., Sharma, M.C., and Finkel, R.C.: Late Quaternary (Holocene) landscape evolution of a monsoon-
407 influenced high Himalayan valley, Gori Ganga, Nanda Devi, NE Garhwal, *Geomorphology*, 61, 91-110,
408 <https://doi.org/10.1016/j.geomorph.2003.12.002>, 2004.

409 Benn, D.I., and Lehmkuhl, F.: Mass balance and equilibrium-line altitudes of glaciers in high-mountain environments, *Quatern.*
410 *Int.*, 65/66, 15-29, [https://doi.org/10.1016/S1040-6182\(99\)00034-8](https://doi.org/10.1016/S1040-6182(99)00034-8), 2000.

411 Bräuning, A.: Tree-ring evidence of ‘Little Ice Age’ glacier advances in southern Tibet, *Holocene*, 16(3), 369-380,
412 <https://doi.org/10.1191/0959683606hl922rp>, 2006.

413 Bueler, E., and Brown, J.: Shallow shelf approximation as a “sliding law” in a thermo mechanically coupled ice sheet model,
414 *J. Geophys. Res-Earth.*, 114, F03008, <https://doi.org/10.1029/2008JF001179>, 2009.

415 Carrivick, J.L., Boston, C.M., King, W., James, W.H., Quincey, D.J., Smith, M.W., Grimes, M., and Evans, J.: Accelerated
416 volume loss in glacier ablation zones of NE Greenland, Little Ice Age to present, *Geophys. Res. Lett.*, 46, 1476–1484,
417 <https://doi.org/10.1029/2018GL081383>, 2019.

418 Chandler, B.M.P., Boston, C.M., and Lukas, S.: A spatially-restricted Younger Dryas plateau icefield in the Gaick, Scotland:
419 Reconstruction and palaeoclimatic implications, *Quaternary. Sci. Rev.*, 211, 107-135,
420 <https://doi.org/10.1016/j.quascirev.2019.03.019>, 2019.

421 Chen, W., Yao, T., Zhang, G., Li, F., Zheng, G., Zhou, Y., and Xu, F.: Towards ice-thickness inversion: an evaluation of global
422 digital elevation models (DEMs) in the glacierized Tibetan Plateau, *The Cryosphere*, 16, 197-281, [https://doi.org/10.5194/tc-16-197-](https://doi.org/10.5194/tc-16-197-2022)
423 [2022](https://doi.org/10.5194/tc-16-197-2022), 2022.

424 Dixit, A., Sahany, S., and Kulkarni, A.V.: Glacial changes over the Himalayan Beas basin under global warming, *J. Environ.*
425 *Manage.*, 295, 113101, <https://doi.org/10.1016/j.jenvman.2021.113101>, 2021.

426 Dong, G., Zhou, W., Yi, C., Fu, Y., Zhang, L., and Li, M.: The timing and cause of glacial activity during the last glacial in
427 central Tibet based on ¹⁰Be surface exposure dating east of Mount Jagang, the Xianza range, *Quaternary. Sci. Rev.*, 186, 284-
428 297, <https://doi.org/10.1016/j.quascirev.2018.03.007>, 2018.

429 Dortch, J.M., Owen, L.A., and Caffee, M.W.: Timing and climatic drivers for glaciation across semi-arid western Himalayan-
430 Tibetan orogen, *Quaternary. Sci. Rev.*, 78, 188-208, <http://dx.doi.org/10.1016/j.quascirev.2013.07.025>, 2013.

431 Eis, J., Maussion, F., and Marzeion, B.: Initialization of a global glacier model based on present-day glacier geometry and past
432 climate information: an ensemble approach, *The Cryosphere*, 13, 3317-3335, <https://doi.org/10.5194/tc-13-3317-2019>, 2019.

433 Farinotti, D., Brinkerhoff, D. J., Clarke, G. K. C., Füst, J. J., Frey, H., Gantayat, P., Gillet-Chaulet, F., Girard, C., Huss, M.,
434 Leclercq, P. W., Linsbauer, A., Machguth, H., Martin, C., Maussion, F., Morlighem, M., Mosbeux, C., Pandit, A., Portmann,
435 A., Rabatel, A., Ramsankaran, R., Reerink, T. J., Sanchez, O., Stentoft, P. A., Singh Kumari, S., van Pelt, W. J. J., Anderson,
436 B., Benham, T., Binder, D., Dowdeswell, J. A., Fischer, A., Helfricht, K., Kutuzov, S., Lavrentiev, I., McNabb, R.,
437 Gudmundsson, G. H., Li, H., and Andreassen, L. M.: How accurate are estimates of glacier ice thickness? Results from ITMIX,
438 the Ice Thickness Models Intercomparison eXperiment, *The Cryosphere*, 11, 949–970, <https://doi.org/10.5194/tc-11-949-2017>,
439 2017.

440 Fu, P., Stroeven, A.P., Harbor, J.M., Hättestrand, C., Heyman, J., Caffee, M.W., and Zhou, P.: Paleoglaciation of Shaluli Shan,
441 southeastern Tibetan Plateau, *Quaternary. Sci. Rev.*, 64, 121-135, <http://dx.doi.org/10.1016/j.quascirev.2012.12.009>, 2013.

442 Furian, W., Maussion, F., and Schneider, C.: Projected 21st-Century Glacial Lake Evolution in High Mountain Asia, *Front.*
443 *Earth. Sci.*, 10, <https://doi.org/10.3389/feart.2022.821798>, 2022.

444 Chevalier, M-L., Hilley, G., Tapponnier, P., Woerd, J.V.D., Liu-Zeng, J., Finkel, R.C., Ryerson, F.J., Li, H., and Liu, X.:
445 Constraints on the late Quaternary glaciations in Tibet from cosmogenic exposure ages of moraine ages. *Quaternary. Sci. Rev.*,
446 30, 528-554, <https://doi.org/10.1016/j.quascirev.2010.11.005>, 2011.

447 Gao, C., Robock, A., Ammann, C.: Volcanic forcing of climate over the past 1500 years: An improved ice core-based index
448 for climate models, *J. Geophys. Res.*, 113, D23111, <https://doi.org/10.1029/2008JD010239>, 2008.

449 Goosse, H., Barriat, P-Y., Dalaiden, Q., Klein, F., Marzeion, B., Maussion, F., Pelucchi, P., and Vlug, A.: Testing the
450 consistency between changes in simulated climate and Alpine glacier length over the past millennium, *Clim. Past.*, 14, 1119-
451 1133, <https://doi.org/10.5194/cp-14-1119-2018>, 2018.

452 Greve, R.: A continuum-mechanical formulation for shallow polythermal ice sheets. *Philos. T.R. Soc. A.*, 355(1726), 921-974,

453 [https://doi.org/10.1175/1520-0442\(1997\)010<0901:AOAPTD>2.0.CO;2](https://doi.org/10.1175/1520-0442(1997)010<0901:AOAPTD>2.0.CO;2), 1997a.

454 Greve, R.: Application of a polythermal three-dimensional ice sheet model to the Greenland ice sheet: Response to steady-
455 state and transient climate scenarios, *J. Climate.*, *10*(5), 901-918, <https://doi.org/10.1098/rsta.1997.0050>, 1997b.

456 Grove, J.M.: *Little Ice Age, 2 ed*, Routledge, 2013.

457 Harris, I., Osborn, T.J., Jones, P., and Lister, D.: Version 4 of the CRU TS monthly high-resolution gridded multivariate climate
458 dataset, *Sci. Data*, *7*, 109, <https://doi.org/10.1038/s41597-020-0453-3>, 2020.

459 Heyman, J.: Paleoglaciation of the Tibetan Plateau and surrounding mountains based on exposure ages and ELA depression
460 estimates, *Quaternary. Sci. Rev.*, *91*, 30-41, <http://dx.doi.org/10.1016/j.quascirev.2014.03.018>, 2014.

461 Heyman, J., Stroeven, A.P., Harbor, J.M., and Caffee, M.W.: Too young or too old: Evaluating cosmogenic exposure dating
462 based on an analysis of compiled boulder exposure ages, *Earth. Planet. Sc. Lett.*, *302*, 71-80,
463 <https://doi.org/10.1016/j.epsl.2010.11.040>, 2011.

464 Hochreuther, P., Loibl, D., Wernicke, J., Zhu, H., Griebinger, J., and Bräuning, A.: Ages of major Little Ice Age glacier
465 fluctuations on the southeast Tibetan Plateau derived from tree-ring-based moraine dating, *Palaeogeogr. Palaeocl.*, *422*, 1-10,
466 <http://dx.doi.org/10.1016/j.palaeo.2015.01.002>, 2015.

467 Jarvis, A., Reuter, H., Nelson, A., and Guevara, E.: Hole-filled SRTM for the globe Version 4, CGIAR Consortium for Spatial
468 Information, University of Twente, 2008.

469 Jeevanjee, N., and Romps, D.M.: Mean precipitation change from a deepening troposphere, *P Natl. Acad. Sci. USA*, *115*(45),
470 11465-11470, <https://doi.org/10.1073/pnas.1720683115>, 2018.

471 Jonathan, C.: Climate change: biological and human aspects. Cambridge University Press. P. 164. ISBN 978-0-521-69619-7,
472 2007.

473 Lifton, N., Sato, T., and Dunai, T.J.: Scaling in situ cosmogenic nuclide production rates using analytical approximations to
474 atmospheric cosmic-ray fluxes, *Earth. Planet. Sc. Lett.*, *386*, 149-160, <http://dx.doi.org/10.1016/j.epsl.2013.10.052>, 2014.

475 Lipscomb, W.H., Price, S.F., Hoffman, M.J., Leguy, G.R., Bennett, A.R., Bradley, S.L., Evans, K.J., Fyke, J.G., Kennedy, J.H.,
476 Perego, M., Ranken, D.M., Sacks, W.J., Salinger, A.G., Vargo, L.J., and Worley, P.J.: Description and evaluating of the
477 Community Ice Sheet Model (CISM) v2.1, *Geosci. Model. Dev.*, *12*, 387-424, <https://doi.org/10.5194/gmd-12-387-2019>, 2019.

478 Liu, J., Yi, C., Li, Y., Bi, W., Zhang, Q., and Hu, G.: Glacial fluctuations around the Karola Pass, eastern Lhagoi Kangri Range,
479 since the Last Glacial Maximum, *J. Quaternary. Sci.*, *32*(4), 516-527, <https://doi.org/10.1002/jqs.2946>, 2017.

480 Lüthi, M.P.: Transient response of idealized glaciers to climate variations, *J. Glaciol.*, *55*(193), 918-903,
481 <https://doi.org/10.3189/002214309790152519>, 2009.

482 Marzeion, B., Jarosch, A. H., and Hofer, M.: Past and future sea-level change from the surface mass balance of glaciers, *The*
483 *Cryosphere*, *6*, 1295–1322, <https://doi.org/10.5194/tc-6-1295-2012>, 2012.

484 Maussion, F., Butenko, A., Champollion, N., Dusch, M., Eis, J., Fourteau, K., Gregor, P., Jarosch, A. H., Landmann, J., Oesterle,

485 F., Recinos, B., Rothenpieler, T., Vlug, A., Wild, C. T., and Marzeion, B.: The Open Global Glacier Model (OGGM) v1.1,
486 *Geosci. Model Dev.*, 12, 909–931, <https://doi.org/10.5194/gmd-12-909-2019>, 2019.

487 Miller, G.H., Geirsdóttir, Á., Zhong, Y., Larsen, D.J., Otto-Bliesner, B.L., Holland, M.M., Bailey, D.A., Refsnider, K.A.,
488 Lehman, S.J., Southon, J.R., Anderson, C., Björnsson, H., and Thordarson, T.: Abrupt onset of the Little Ice Age triggered by
489 volcanism and sustained by sea-ice/ocean feedbacks, *Geophys. Res. Lett.*, 39, L02708, <https://doi.org/10.1029/2011GL050168>,
490 2012.

491 Murari, M.K., Owen, L.A., Dortch, J.M., Caffee, M.W., Dietsch, C., Fuchs, M., Haneberg, W.C., Sharma, M.C., and Townsend-
492 Small, A.: Timing and climatic drivers for glaciation across monsoon-influenced regions of the Himalayan-Tibetan orogen,
493 *Quaternary. Sci. Rev.*, 88, 159-182, <http://dx.doi.org/10.1016/j.quascirev.2014.01.013>, 2014.

494 Oerlemans, J., Anderson, B., Hubbard, A., Huybrechts, Ph., Jóhannesson, T., Knap, W.H., Schmeits, M., Stroeven, A.P., van
495 de Wal, R.S.W., and Zuo, Z.: Modelling the response of glaciers to climate warming, *Climate Dynamics*, 14, 267-274,
496 <https://doi.org/10.1007/s003820050222>, 1998.

497 Owen, L.A.: Latest Pleistocene and Holocene glacier fluctuations in the Himalaya and Tibet, *Quaternary. Sci. Rev.*, 28, 2150-
498 2164, <https://doi.org/10.1016/j.quascirev.2008.10.020>, 2009.

499 Owen, L.A., and Dortch, J.M.: Nature and timing of Quaternary glaciation in the Himalayan-Tibetan orogen, *Quaternary. Sci.*
500 *Rev.*, 88, 14-54, <http://dx.doi.org/10.1016/j.quascirev.2013.11.016>, 2014.

501 PAGES 2k-PMIP3 group.: Continental-scale temperature variability in PMIP3 simulations and PAGES 2k regional
502 temperature reconstructions over the past millennium, *Clim. Past.*, 11, 1673-1699, <https://doi.org/10.5194/cp-11-1673-2015>,
503 2015.

504 Parkes, D., and Goosse, H.: Modelling regional glacier length changes over the last millennium using the Open Global Glacier
505 Model, *The Cryosphere*, 14, 3135-3153, <https://doi.org/10.5194/tc-14-3135-2020>, 2020.

506 Pelto, B.M., Maussion, F., Menounos, B., Radić, V and Zeuner, M.: Bias-corrected estimates of glacier thickness in the
507 Columbia River Basin, Canada, *J. Glaciol.*, 66(260), 1051-1063, <https://doi.org/10.1017/jog.2020.75>, 2020.

508 Peng, X., Chen Y., Liu, G., Liu, B., Li, Y., Liu, Q., Han, Y., Yang, W., and Cui, Z.: Late Quaternary glaciations in the Cogarbu
509 valley, Bhutanese Himalaya, *J. Quaternary. Sci.*, 34(1), 40-50, <http://dx.doi.org/10.1002/jqs.3079>, 2019.

510 Peng, X., Chen, Y., Li, Y., Liu, B., Liu, Q., Yang, W., Liu, G.: Late Holocene glacier fluctuations in the Bhutanese Himalaya,
511 *Global. Planet. Change.*, 187, 103137, <https://doi.org/10.1016/j.gloplacha.2020.103137>, 2020.

512 Pronk, J.B., Bolch, T., King, W., Wouters, B., and Benn, D.I.: Contrasting surface velocities between lake- and land-terminating
513 glaciers in the Himalayan region, *The Cryosphere*, 15, 5577-5599, <https://doi.org/10.5194/tc-15-5577-2021>, 2021.

514 Qiao, B., and Yi, C.: Reconstruction of Little Ice Age glacier area and equilibrium line attitudes in the central and western
515 Himalaya, *Quatern. Int.*, 444, 65-75, <http://dx.doi.org/10.1016/j.quaint.2016.11.049>, 2017.

516 Qureshi, M.A., Li, Y., Yi, C., and Xu, X.: Glacial changes in the Hunza Basin, western Karakoram, since the Little Ice Age,

517 *Palaeogeogr. Palaeocl.*, 562, 110086, <https://doi.org/10.1016/j.palaeo.2020.110086>, 2021.

518 Rampino, M.R., and Self, S.: Historic Eruptions of Tambora (1815), Krakatau (1883), and Agung (1963), their Stratospheric
519 Aerosols, and Climatic Impact, *Quatern. Res.*, 18, 127-143, [https://doi.org/10.1016/0033-5894\(82\)90065-5](https://doi.org/10.1016/0033-5894(82)90065-5), 1982.

520 RGI Consortium.: Randolph Glacier Inventory (RGI)-A Dataset of Global Glacier Outlines: Version 6.0,
521 <https://doi.org/10.7265/N5-RGI-60>, 2017.

522 Saha, S., Owen, L.A., Orr, E.N., and Caffee, M.W.: High-frequency Holocene glacier fluctuations in the Himalayan-Tibetan
523 orogen, *Quaternary. Sci. Rev.*, 220, 372-400, <https://doi.org/10.1016/j.quascirev.2019.07.021>, 2019.

524 Saha, S., Owen, L.A., Orr, E.N., & Caffee, M.W.: Timing and nature of Holocene glacier advances at the northwestern end of
525 the Himalayan-Tibetan orogen, *Quaternary. Sci. Rev.*, 187, 177-202, <https://doi.org/10.1016/j.quascirev.2018.03.009>, 2018.

526 Schmidt, G. A., Jungclaus, J. H., Ammann, C. M., Bard, E., Braconnot, P., Crowley, T. J., Delaygue, G., Joos, F., Krivova,
527 N.A., Muscheler, R., Otto-Bliesner, B.L., Pongratz, J., Shindell, D.T., Solanki, S.K., Steinhilber, F., and Vieira, L.E.A.: Climate
528 forcing reconstructions for use in PMIP simulations of the last millennium (v1.0), *Geosci. Model. Dev.*, 4, 33-45,
529 <https://doi.org/10.5194/gmd-4-33-2011>, 2011.

530 Shafeeque, M., and Luo, Y.: A multi-perspective approach for selecting CMIP6 scenarios to project climate change impacts on
531 glacio-hydrology with a case study in Upper Indus River basin, *J. Hydrol.*, 599, 126466,
532 <https://doi.org/10.1016/j.jhydrol.2021.126466>, 2021.

533 Sigdel, S.R., Zhang, H., Zhu, H., Muhammad, S., and Liang, E.: Retreating glacier and advancing forest over the past 200
534 years in the Central Himalayas, *J. Biogeogr.*, 125, e2020JG005751. <https://doi.org/10.1029/2020JG005751>, 2020.

535 Solomina, O.N., Bradley, R.S., Hodgson, D.A., Ivy-Ochs, S., Jomelli, V., Mackintosh, A.N., Nesje, A., Owen, L.A., Wanner,
536 H., Wiles, G.C., and Young, N.E.: Holocene glacier fluctuations, *Quaternary. Sci. Rev.*, 111, 9-34,
537 <http://dx.doi.org/10.1016/j.quascirev.2014.11.018>, 2015.

538 Taylor, K., Stouffer, R., and Meehl, G.: An Overview of CMIP5 and the Experiment Design, *B. Am. Meteorol. Soc.*, 93, 485-
539 498, <https://doi.org/10.1175/BAMS-D-11-00094.1>, 2012.

540 Winkelmann, R., Martin, M.A., Haseloff, M., Albrecht, T., Bueler, E., Khroulev, C., and Levermann, A.: The Potsdam Parallel
541 Ice Sheet Model (PISM-PIK) – Part 1: Model description, *The Cryosphere*, 5, 715-726, <https://doi.org/10.5194/tc-5-715-2011>,
542 2011.

543 Xu, X., and Yi, C.: Little Ice Age on the Tibetan Plateau and its bordering mountains: Evidence from moraine chronologies,
544 *Global. Planet. Change.*, 116, 41-53, <http://dx.doi.org/10.1016/j.gloplacha.2014.02.003>, 2014.

545 Yan, Q., Owen, L. A., Wang, H., and Zhang, Z.: Climate constraints on glaciation over High-Mountain Asia during the last
546 glacial maximum, *Geophys. Res. Lett.*, 45, 9024–9033, <https://doi.org/10.1029/2018GL079168>, 2018.

547 Yan, Q., Owen, L. A., Zhang, Z., Wang, H., Wei, T., Jiang, N., and Zhang, R.: Divergent evolution of glaciation across High-
548 Mountain Asia during the last four glacial-interglacial cycles, *Geophys. Res. Lett.*, 48, e2021GL092411,
20

549 <https://doi.org/10.1029/2021GL092411>, 2021.

550 Yan, Q., Owen, L.A., Zhang, Z., Jiang, N., and Zhang, R.: Deciphering the evolution and forcing mechanisms of glaciation
551 over the Himalayan-Tibetan orogen during the past 20,000 years, *Earth. Planet. Sc. Lett.*, *541*, 116295,
552 <https://doi.org/10.1016/j.epsl.2020.116295>, 2020.

553 Yang, B., Achim, B., and Shi, Y.: Late Holocene temperature fluctuations on the Tibetan Plateau, *Quaternary. Sci. Rev.*, *22*,
554 2335-2344, [https://doi.org/10.1016/S0277-3791\(03\)00132-X](https://doi.org/10.1016/S0277-3791(03)00132-X), 2003.

555 Yi, C., Chen, H., Yang, J., Liu, B., Fu, P., Liu, K., and Li, S.: Review of Holocene glacial chronologies based on radiocarbon
556 dating in Tibet and its surrounding mountains, *J. Quaternary. Sci.*, *23(6-7)*, 533-543, <https://doi.org/10.1002/jqs.1228>, 2008.

557 Zekollari, H., and Huybrechts, P.: On the climate–geometry imbalance, response time and volume–area scaling of an alpine
558 glacier: insights from a 3-D flow model applied to Vadret da Morteratsch, Switzerland, *Ann. Glaciol.*, *56(70)*, 51-62,
559 <https://doi.org/10.3189/2015AoG70A921>, 2015.

560 Zhang, Q., Yi, C., Dong, G., Fu, P., Wang, N., and Capolongo, D.: Quaternary glaciations in the Lopu Kangri area, central
561 Gangdise Mountains, southern Tibetan Plateau, *Quaternary. Sci. Rev.*, *201*, 470-482,
562 <https://doi.org/10.1016/j.quascirev.2018.10.027>, 2018a.

563 Zhang, Q., Yi, C., Fu, P., Wu, Y., Liu, J., and Wang, N.: Glacier change in the Gangdise Mountains, southern Tibet, since the
564 Little Ice Age, *Geomorphology*, *306*, 51-63, <https://doi.org/10.1016/j.geomorph.2018.01.002>, 2018b.